Large-scale state-dependent membrane remodeling by a transporter protein

W. Zhou[1], G. Fiorin[1], C. Anselmi[1,3], H.A. Karimi-Varzaneh[2,4], H. Poblete[1,2,5], L.R. Forrest[2]*, J.D. Faraldo-Gómez[1]*

[1]Theoretical Molecular Biophysics Laboratory, National Heart, Lung & Blood Institute
National Institutes of Health, Bethesda, MD

[2]Computational Structural Biology Section, National Institute of Neurological Disorders & Stroke
National Institutes of Health, Bethesda, MD

[3]Present address: Children's National Hospital, Washington, DC

[4]Present address: Continental Reifen Deutschland GmbH, Hannover, Germany

[5]Present address: Centro de Bioinformática y Simulación Molecular, University of Talca, Chile

* To whom correspondence should be addressed:

Dr. Lucy R. Forrest,
35 Convent Drive, Room 3D991, Bethesda, MD 20892-3761, USA
E-mail: lucy.forrest@nih.gov, Telephone: (301) 402-2012

&

Dr. José D. Faraldo-Gómez,
10 Center Drive, Room 5N307, Bethesda, MD 20892, USA
E-mail: jose.faraldo@nih.gov, Telephone: (301) 827-0821

Abstract

That channels and transporters can influence the membrane morphology is increasingly recognized. Less appreciated is that the extent and free-energy cost of these deformations likely varies among different functional states of a protein, and thus, that they might contribute significantly to defining its mechanism. We consider the trimeric Na^+-aspartate symporter Glt_{Ph}, a homolog of an important class of neurotransmitter transporters, whose mechanism entails one of the most drastic structural changes known. Molecular simulations indicate that when the protomers become inward-facing, they cause deep, long-ranged, and yet mutually-independent membrane deformations. Using a novel simulation methodology, we estimate that the free-energy cost of this membrane perturbation is in the order of 6-7 kcal/mol per protomer. Compensating free-energy contributions within the protein or its environment must thus stabilize this inward-facing conformation for the transporter to function. We discuss these striking results in the context of existing experimental observations for this and other transporters.

Introduction

Integral membrane proteins can have a marked impact on the morphology of the surrounding bilayer. For example, they might alter its curvature or thickness, or foster the enrichment or depletion of specific types of lipid in their vicinity (Lee, 2004; Andersen, 2007; Marsh, 2008; Phillips, 2009). These perturbations develop to accommodate the amino-acid composition and specific structural features of the protein surface. For a broad range of systems of interest, however, these features are not static, but vary as the protein carries out its biological activity. Examples include channel proteins and their gating mechanisms, or the conformational cycles resulting in alternating access in active transporters. The protein-lipid interface also changes when membrane proteins form complexes or oligomers. Because most membrane perturbations entail an energetic or entropic cost, it seems reasonable to expect that the bilayer contributes to the thermodynamics and kinetics of these processes, favoring or disfavoring specific structural states. Such interdependence would help explain why changes in lipid bilayer composition, either resulting from natural regulatory mechanisms or induced artificially, can have a determining effect on protein function (Jensen, 2004; Andersen, 2007; Denning, 2013; Cordero-Morales, 2018; Haselwandter, 2018).

Here, we seek to gain insights into this interplay for a class of membrane proteins known to undergo a striking structural transformation, namely secondary-active transporters featuring the so-called elevator mechanism. We specifically focus on the Na^+-aspartate symporter Glt_{Ph} from *Pyrococcus horikoshii*, a member and model system of the Excitatory Amino-Acid Transporter (EAAT) family, which includes the human SLC1 neurotransmitter transporters (Gether, 2006). Secondary-active transporters like Glt_{Ph} interconvert between two major conformational states that alternately expose binding sites for ions and substrate to either side of the membrane (**Fig. 1**) (Jardetzky, 1966; Reyes, 2009; Boudker, 2010; Forrest, 2011). In Glt_{Ph}, this conformational interconversion takes place only when Na^+ and aspartate occupy the transporter or when the transporter is empty (Yernool, 2004; Boudker, 2007; Ryan, 2009), which defines this protein as a co-transporter. For either occupancy state, the exchange between outward- and inward-facing conformations is spontaneous, i.e., it does not require an extrinsic electrochemical driving force. However, the relative populations of these conformational states and the net directionality of the transport cycle do depend on the membrane potential and the relative concentrations of ions and substrates on either side of the membrane. This dependence is why downhill translocation of Na^+ will power uphill transport of aspartate, and vice versa.

Glt_{Ph} forms a homotrimer (Yernool, 2004); yet, each protomer works independently from its neighbors (Akyuz, 2013; Erkens, 2013; Akyuz, 2015; Ruan, 2017). The protomers consist of two distinct units: the scaffold domain, which provides a stable trimerization interface (Groeneveld, 2007; Verdon, 2012; Georgieva, 2013; Hänelt, 2013), and the transport domain, which encapsulates the ion and aspartate binding sites (Yernool, 2004; Reyes, 2009). Both domains are exposed to the lipid bilayer, but structures of Glt_{Ph} in outward- and inward-facing states clearly reveal that it is the movement of the latter domain that results in alternating access (Yernool, 2004; Reyes, 2009). Specifically, if one assumes that the scaffold domains remain stationary relative to the membrane mid-plane, each transport domain would move

perpendicularly to that plane by approximately 15 Å, i.e., about one-third of the total bilayer width. How this drastic structural change impacts the relationship between protein and membrane has, to our knowledge, not been previously evaluated. One might envisage that the transport domains simply traverse the membrane (as an elevator), moving polar sidechains on their surface into the bilayer interior and exposing hydrophobic ones to the solvent (Reyes, 2009). Alternatively, the morphology of the lipid bilayer could adapt to the conformational state of the protein, and match the amino-acid make-up of the protein surface throughout the transport cycle. Which of these two possibilities entails the least energetic cost is entirely unclear. The absence of functional cooperativity among protomers would appear to rule out the latter, as a pronounced membrane deformation induced by one protomer could impact the conformational dynamics of its two neighbors. On the other hand, the cumulative cost of dehydration of polar and charged sidechains could be exceedingly large. Experimental studies of the Glt_{Ph} homolog EAAT2 also appear to show that bilayer-facing regions in the outward-facing state are similarly solvent-accessible throughout the transport cycle (Silverstein, 2013).

Molecular dynamics simulations in principle provide a means to examine this interplay in great detail (Cui, 2013; Marrink, 2019). Current computing power makes it feasible to examine the morphology of simple phospholipid membranes around protein structures, for many cases of interest. Highly complex membranes remain beyond reach, however, if represented in atomic detail, as the relaxation time of an arbitrarily-configured multi-component lipid mixture is slower than typically attainable simulation times, thus imposing a starting-condition bias on any analysis. In such cases, so-called coarse-grained simulations are a viable approach despite their reduced level of detail (Corradi, 2018). By contrast, simulation methods that permit a direct quantification of the energetic footprint of a membrane morphological change have been lacking. Computational approaches in this area have typically relied on continuum-mechanics theories of membrane elasticity, which necessarily pre-suppose important parameters defining the bilayer energetics (Argudo, 2017). Although such approaches can be predictive and insightful in some cases (Mondal, 2011; Bethel, 2016), it is unclear whether macroscopic models are generally transferable to the length-scales of individual membrane proteins (Lee, 2013; Fiorin, 2019). To circumvent this problem, we have recently developed a free-energy simulation method (Fiorin, 2019) with which the potential-of-mean-force of a membrane deformation can be probed directly from a simulation system, much in the same way processes such as ligand recognition or ion permeation are commonly characterized. Here, in addition to conventional simulations and structural bioinformatic approaches, we apply this new technology to obtain quantitative insights into the nature of the interplay between Glt_{Ph} and the surrounding membrane. The implications of the major conformational change required for transport are discussed in the light of available experimental observations.

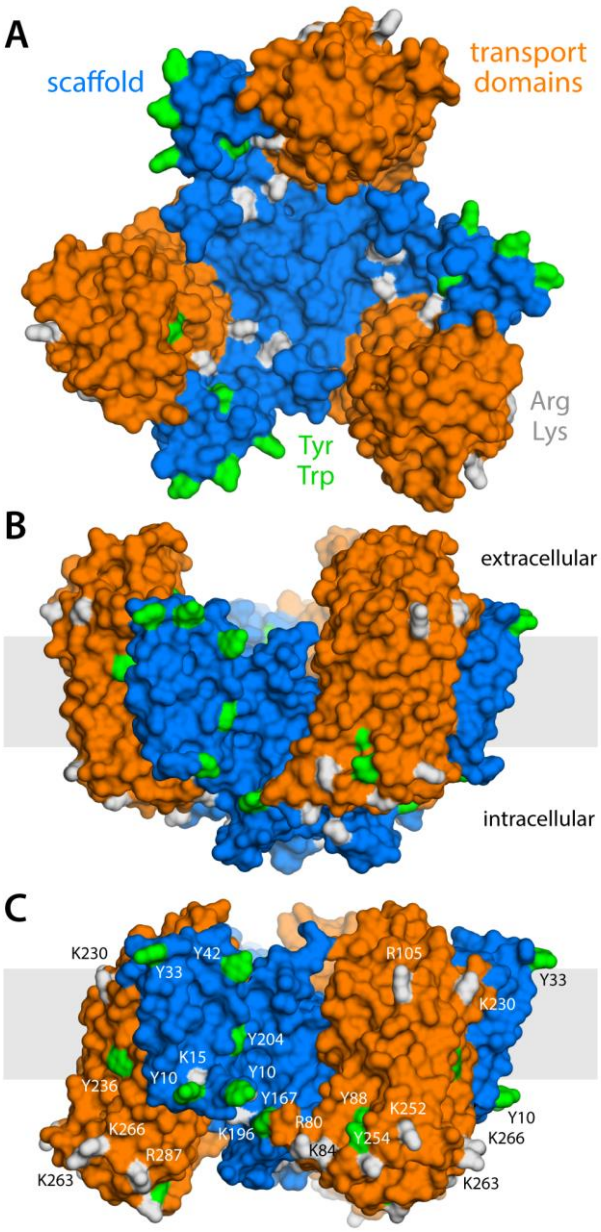

Figure 1. Structure of the Glt_{Ph} trimer in the outward- and inward-facing states. (**A**) View from the extracellular space, with the 3 protomers in the outward-facing conformation (PDB 2NWL). The 'scaffold' (blue) mediates all protein-protein interactions between protomers. The 'transport' domains (orange) carry the bound substrates, moving relative to the scaffold perpendicularly to the membrane. (**B**) Same as (A), viewed along the membrane plane, with the approximate membrane region shown as a gray box. Side-chains that might interact with lipid headgroups are highlighted (Tyr, Trp, Arg, Lys). (**C**) Same view as (B), with all three protomers in the inward-facing conformation (PDB 3KBC).

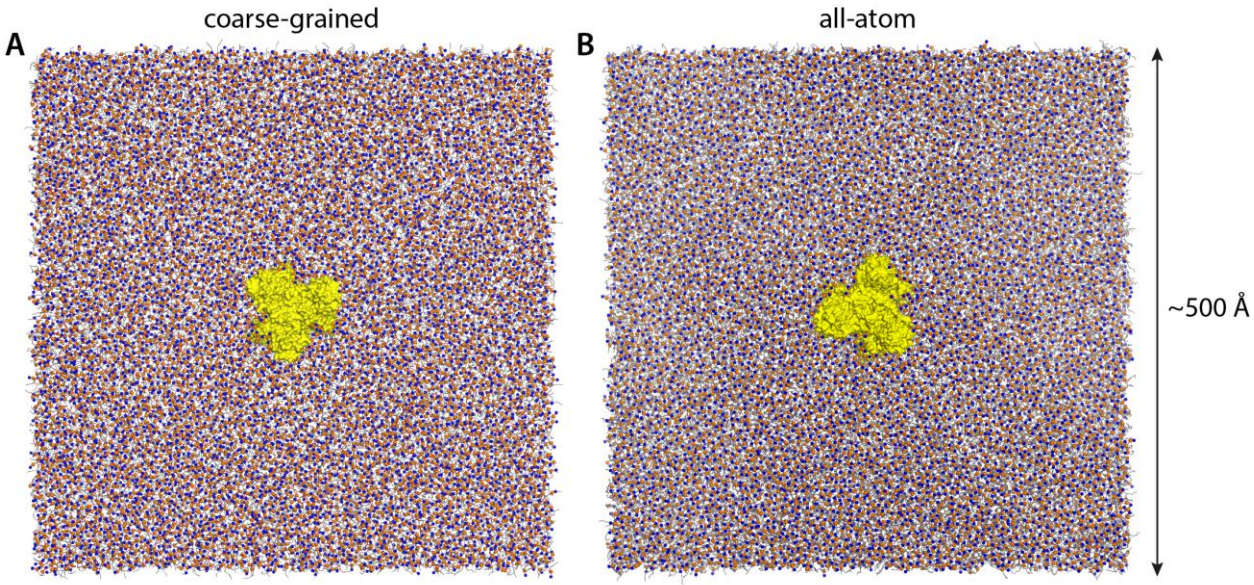

Figure 1 – figure supplement 1. Molecular simulation systems. (**A**) Coarse-grained representation of all-inward Glt_{Ph} (yellow surface) in a model POPC membrane (298 K), viewed from the extracellular space. Phosphate and choline groups are highlighted with orange and blue spheres, respectively. The system amounts to ~260,000 particles, including ~7,500 lipid molecules. Analogous simulation systems were constructed to study states of Glt_{Ph} with one, two or all three protomers in the outward-facing conformation. (**B**) All-atom representation of all-inward Glt_{Ph}, in a DPPC membrane (323 K). This simulation system amounts to ~3,000,000 atoms. Note that the longest dimension of the Glt_{Ph} trimer is ~80 Å. The solvent is omitted in both panels, for clarity.

Results

Alternating access causes major membrane deformations, long-ranged but non-cooperative

To examine how the transport cycle of Glt_{Ph} impacts the surrounding membrane, we carried out molecular dynamics simulations of phospholipid bilayers containing structures of Glt_{Ph} trimers in four different conformational states. Specifically, we examined states where all three protomers are in either the inward- or outward-facing states (**Fig. 1**), as well as two intermediates where one protomer is inward-facing and the other two are outward-facing, or vice versa. To enable the calculations to reveal long-range perturbations, the simulated membranes are about 50×50 nm^2 in size, i.e., six-fold wider than the transporter (**Fig. 1 – fig. suppl. 1**). This area translates into ~7,500 lipid molecules, much larger than typical simulation systems. In a first set of calculations, therefore, we opted for coarse-grained representation of the molecular system, using the MARTINI forcefield (Marrink, 2007; Monticelli, 2008). The conformational state of the trimer was preserved throughout each of the simulations, while the lipid bilayer was free to adjust to that state. It is worth noting that the elastic properties of lipid bilayers, as quantified by, e.g., their macroscopic bending modulus, are well described by MARTINI, despite its inherent approximations (Marrink, 2004; Fiorin, 2019).

The results of this analysis are summarized in **Fig. 2**. For the state with all three protomers in the outward-facing conformation, we found the membrane to be only modestly perturbed. This perturbation is maximal in the vicinity of the transport domains, where the membrane mid-plane is elevated by 3-4 Å; near the scaffold, however, the elevation is only ~2 Å. By contrast, for the cases in which one, two or all three transport domains are in the inward-facing state, we observe a major morphological impact on the surrounding membrane. Specifically, we observe that the displacement of the transport domain causes a ~10 Å depression in the lipid bilayer, i.e., about 50% of the width of its hydrophobic core. This perturbation is also remarkably long-ranged, extending radially for nearly 100 Å from the protein surface (**Fig. 2D**). Strikingly, however, along the perimeter of the protein, the perturbation is entirely confined to the interface with the transport domain, i.e., it is abruptly terminated near the scaffold, where the membrane is again minimally depressed, by only about 1-2 Å. Indeed, comparison of intermediates with one or two protomers in the inward-facing state shows that each transport domain causes an independent perturbation, largely identical and seemingly additive to that caused by the other protomers, while in the vicinity of the scaffold domains the membrane remains largely unperturbed.

The data presented in **Fig. 2** were obtained for a POPC membrane under no tension (Methods). Similar results were obtained in simulations with applied membrane tensions as high as 10 mN/m (**Fig. 3**), and in simulations with bilayers of different composition, namely either POPE, a 2:1 mixture of POPE and POPG (both at 298 K), and DPPC (at 323 K) (**Fig. 4**). It should also be noted that the observed deflections in the membrane mid-plane do not result from significant differences in lipid-bilayer thickness (**Fig. 4 – fig. suppl. 1**). Analysis of the second-rank order parameter of the lipid alkyl tails, which is a measure of their tilt relative to the membrane perpendicular, also shows little contrast between the outward- and inward-facing conformational states (**Fig. 4 – fig. suppl. 2**). The only significant difference is observed for the inner leaflet, at the point where the transport domain meets the scaffold, in the inward-facing

state. Here, the lipids become significantly tilted, on average, seemingly to adapt to the abrupt changes in membrane curvature induced by the transport domains. This effect is, however, localized and does not propagate beyond the perimeter of the scaffold. We conclude, therefore, that the long-ranged deformations induced by Glt_{Ph} are most accurately described as bending, rather than other types of perturbation.

Finally, it is interesting to note that our simulations show that the trimerization domain is not completely static relative to the membrane throughout the alternating-access cycle; as indicated in **Fig. 2D**, we observe that the scaffold shifts by about 2 Å when the all-outward and all-inward states are compared. Consequently, the vertical displacement of the transport domains relative to the membrane is slightly larger than the ~15 Å that would be deduced from an overlay of the structures.

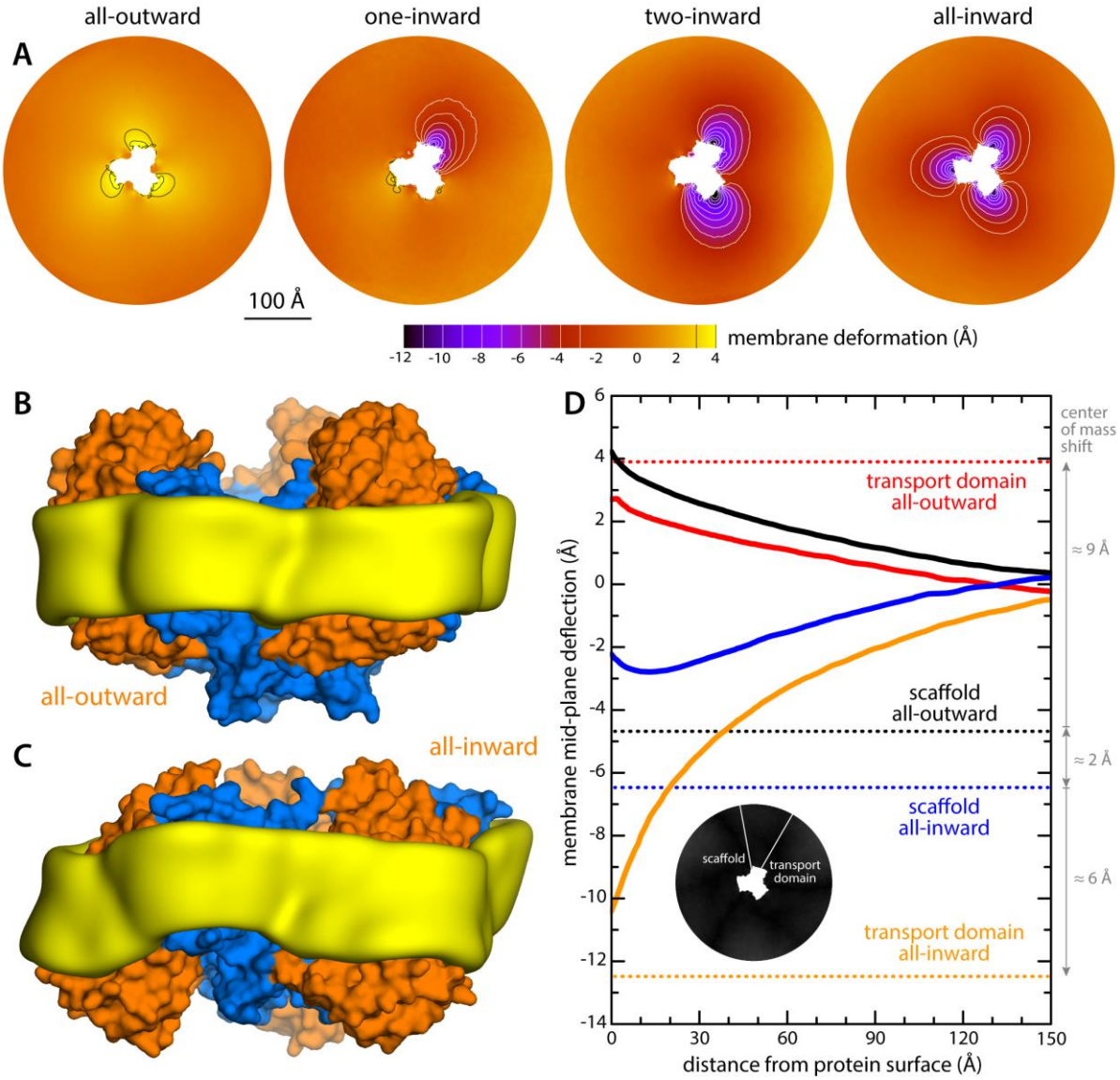

→ **Figure 2.** Changes in membrane morphology induced by the conformational cycle of Glt_{Ph}. The results are based on coarse-grained MD simulations of the transporter in a POPC bilayer at 298K. (**A**) Deflection of the membrane mid-plane, for each of the primary states in the cycle. The deflection is quantified by calculating the mean value of the *Z* coordinate of the bilayer across the *X*-*Y* plane. The zero-level is set at ~200 Å from the protein center, where the membrane mid-plane is flat, on average. The resulting maps are viewed from the extracellular space. Each map is the mean of *N* = 3 observations, each of which is a time-average for one simulated trajectory. Positive values reflect an outward deflection; negative values reflect inward bending. Values equal to or greater than ± 3 Å are contoured (black/white), for clarity. From left to right, the standard error of the data across each map is, on average, 0.8 Å, 0.8 Å, 0.5 Å and 0.6 Å. (**B**) Structure of all-outward Glt_{Ph} (represented as in Fig. 1), alongside a calculated density map for the lipid bilayer alkyl chains within 10 Å of the protein surface (yellow), based on all simulation data gathered for this state. See also Video 1. (**C**) Same as (B), for the all-inward state. See also Video 2. (**D**) Cross-sections of the membrane-deflection data in (A), plotted as a function of the distance to the protein surface. The cross-sections project away from the transport domain, in either the all-outward or all-inward states (solid red and orange lines, respectively), or from the scaffold domain (solid black and blue lines, respectively), following the direction indicated by the inset schematic. Horizontal dashed lines indicate the location of the center of mass of each domain, in either conformation (same color scheme).

Video 1. Changes in membrane morphology induced by the conformational cycle of Glt_{Ph}. Structure of all-outward Glt_{Ph} (represented as in Fig. 1) alongside a calculated density map for the lipid bilayer alkyl chains within 10 Å of the protein surface (yellow), based on CG simulations for this state in a POPC membrane.

Video 2. Changes in membrane morphology induced by the conformational cycle of Glt_{Ph}. Structure of all-inward Glt_{Ph} (represented as in Fig. 1) alongside a calculated density map for the lipid bilayer alkyl chains within 10 Å of the protein surface (yellow), based on CG simulations for this state in POPC membrane.

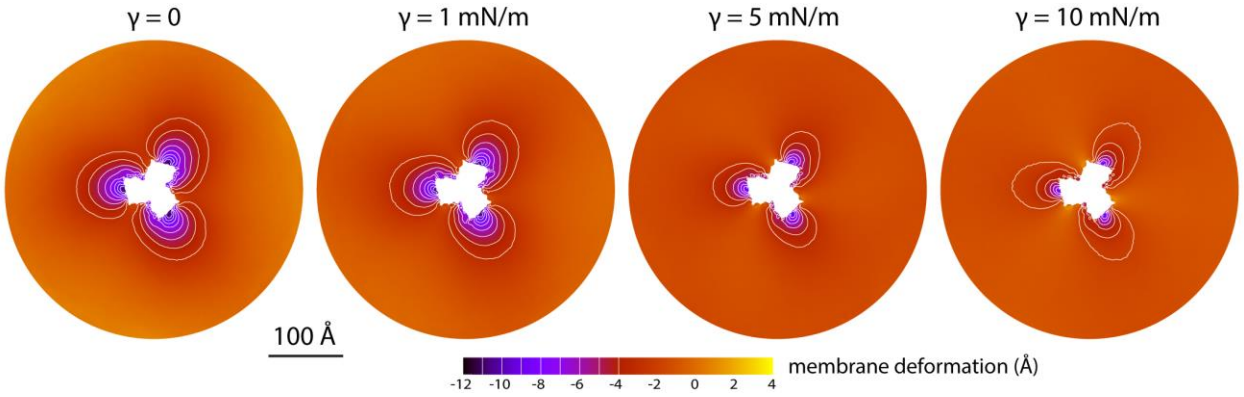

Figure 3. Membrane deformation induced by all-inward Glt_{Ph} in coarse-grained MD simulations in a POPC bilayer at 298 K, with and without an applied membrane tension of increasing magnitude (as indicated). The deflection of the membrane mid-plane was calculated and represented as in Fig. 2A. From left to right, the standard error of the data (*N* = 3) across each map is, on average, 0.6 Å, 0.7 Å, 0.4 Å and 0.3 Å.

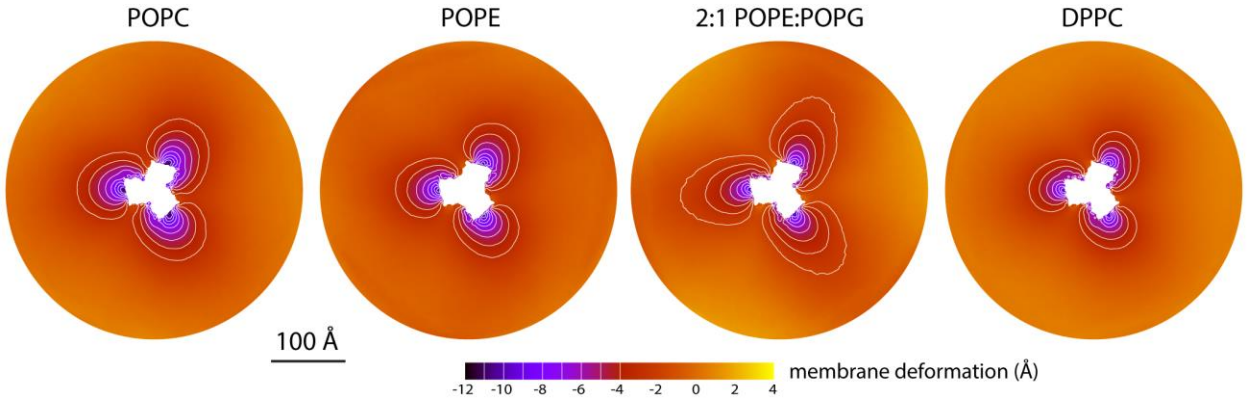

Figure 4. Membrane deformation induced by all-inward Glt_{Ph} in coarse-grained MD simulations in different bilayers. The data for POPC, POPE, and 2:1 POPE:POPG were obtained at 298 K; the data for DPPC were obtained at 323 K. The deflection of the membrane mid-plane was calculated and represented as in Fig. 2A. From left to right, the standard error of the data (*N* = 3) across each map is, on average, 0.6 Å, 0.6 Å, 0.4 Å and 1.0 Å.

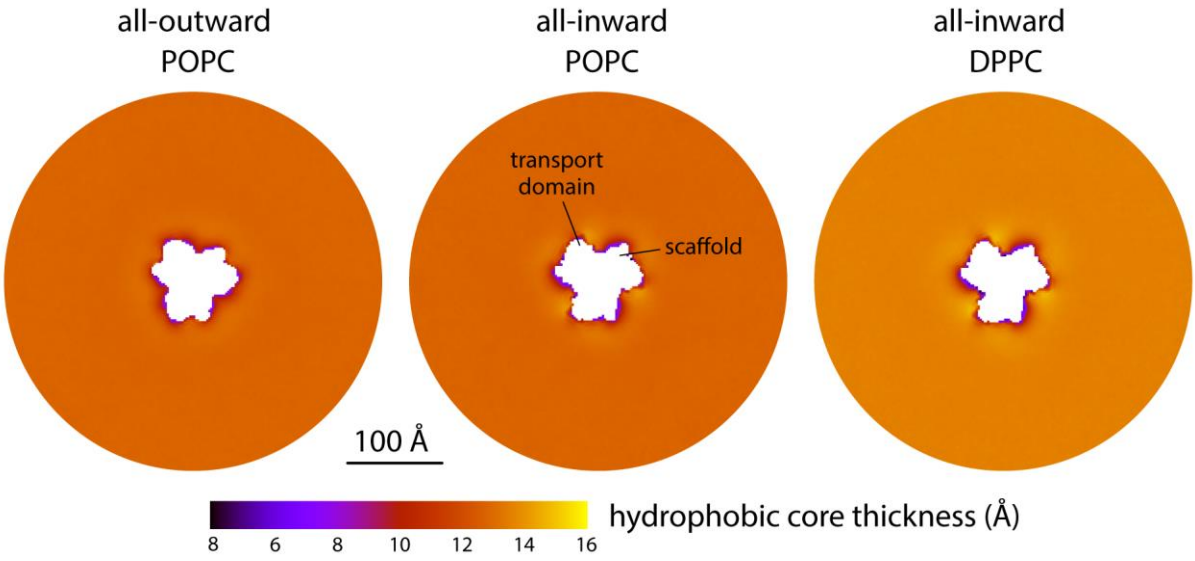

Figure 4 – figure supplement 1. Changes in membrane morphology induced by the conformational cycle of Glt_{Ph}. The plots quantify the thickness of the hydrophobic core of the membrane, as defined by the lipid alkyl chains, in either the all-outward or all-inward states of the transporter. Data are shown for coarse-grained simulations in POPC at 298 K and in DPPC at 323 K. Similarly to Fig. 2A, each map reflects the mean of *N* = 3 time-averages derived from independent simulation trajectories.

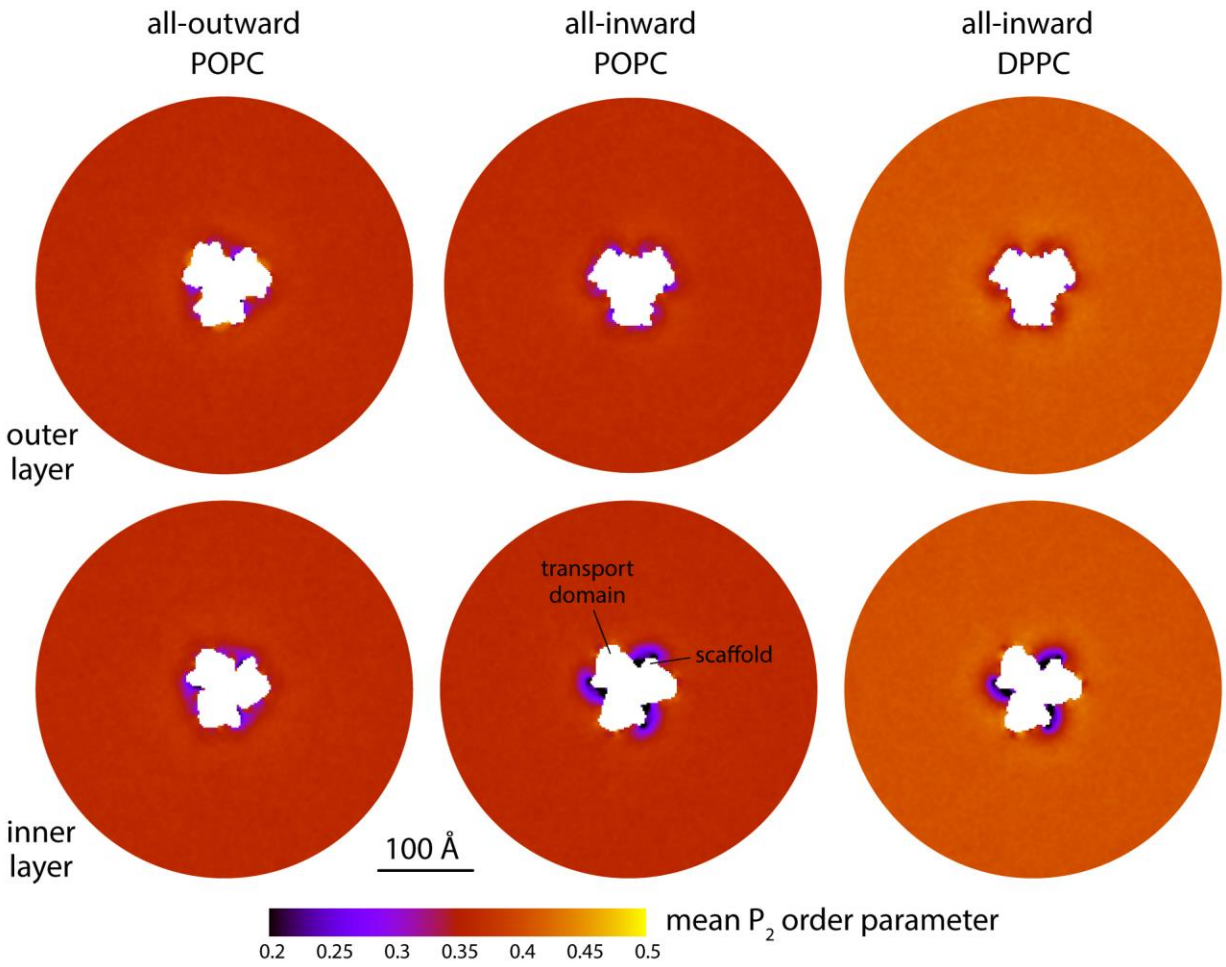

Figure 4 – figure supplement 2. Changes in membrane morphology induced by the conformational cycle of Glt_{Ph}. The plots quantify the mean second-rank order parameter of the C-C bonds along the lipid alkyl chains, for either the outer or inner layers of the lipid bilayer (upper and lower panels, respectively), in either the all-outward or all-inward state of the transporter. The second-rank order parameter of a given C-C bond along the chain is defined as $1/2\ (3\cos^2\langle\theta\rangle - 1)$, where $\langle\theta\rangle$ denotes the average value of the angle between the bond and the bilayer normal. Data are shown for coarse-grained simulations in POPC at 298 K and in DPPC at 323 K. Similarly to Fig. 2A, each map reflects the mean of $N = 3$ time-averages derived from independent simulation trajectories.

Transport domains bend the membrane, while scaffold domains anchor it

Although the coarse-grained MARTINI forcefield yields a reasonably accurate description of membrane elasticity (Marrink, 2004; Fiorin, 2019), the degree to which it also captures the specificity of bi-molecular interactions has been questioned (Javanainen, 2017). We thus considered the possibility that the nature of the membrane deformations observed for the inward-facing conformation of Glt_{Ph} results from the lack of sufficient detail in the representation of protein and lipid structures and their interactions. To address this concern, we carried out three independent simulations of the all-inward state, using the all-atom CHARMM forcefield (see Methods). Each trajectory was initialized with a different starting condition, derived from the previous coarse-grained simulations. The simulation systems are therefore identical in size to those described above. Of course, the computational cost is much greater, as the simulation system now amounts to ~3,000,000 atoms (**Fig. 1 – fig. suppl. 1B**).

Reassuringly, the results obtained with the all-atom representation recapitulate those obtained with the coarse-grained forcefield (**Fig. 5**). Even after a suitable relaxation time following the change in forcefield (**Fig. 5 – fig. suppl. 1AB**), and despite a significant number of exchanges between lipids in the bulk and near the protein surface (**Fig. 5 – fig. suppl. 1C**), the deformations induced by the transport domains were sustained in both magnitude and range; the abrupt restoration of membrane shape at the scaffold-domain interface also continued to be observed.

What might explain these striking effects? The complementary analyses described in **Fig. 5C** and **Fig. 6** indicate that the membrane adapts to the conformational state of the protein to preclude strongly hydrophilic side chains from penetrating the core of the bilayer, while also avoiding exposure of hydrophobic portions of the protein surface to solvent. The deformed state of the bilayer also appears to be stabilized by numerous hydrogen-bonding interactions between polar and aromatic residues and lipid headgroups. For example, it is apparent that Arg105 and Lys230, which face the extracellular solution in the outward-facing state (**Fig. 1**), would be fully dehydrated in the inward-facing conformation were it not for the fact that the membrane bends inwards (**Fig. 6C**). Instead, these residues form highly persistent interactions with the phosphate and ester groups in the lipid bilayer (**Fig. 5C**). Conversely, a large number of hydrophobic residues on the intracellular side of the transport domain would be exposed to solvent if the membrane was unchanged (**Fig. 6C**). As illustrated in **Fig. 6B** (and **Fig. 6 – Suppl. 1B**) individual per-residue preferences accumulated across the protein surface add up to very large energetic gains (which, as will be discussed later, are balanced by the resistance of the membrane to be deformed). Notably, this pattern of H-bonding interactions extends to the scaffold, where they appear to help anchor the bilayer in between adjacent transport domains, on both sides of the membrane (**Fig. 5C**). Interestingly, clear co-evolutionary relationships can be detected across Glt_{Ph} homologs for several clusters of membrane-exposed residues that include those engaged in hydrogen-bonding with lipids in our simulations (**Fig. 6D**). In summary, the changes in membrane morphology induced by the conformational cycle of Glt_{Ph} thus appear to be dictated by the displacement of protein interfaces that have evolved to be closely matched with the chemical features of the membrane and the surrounding solvent.

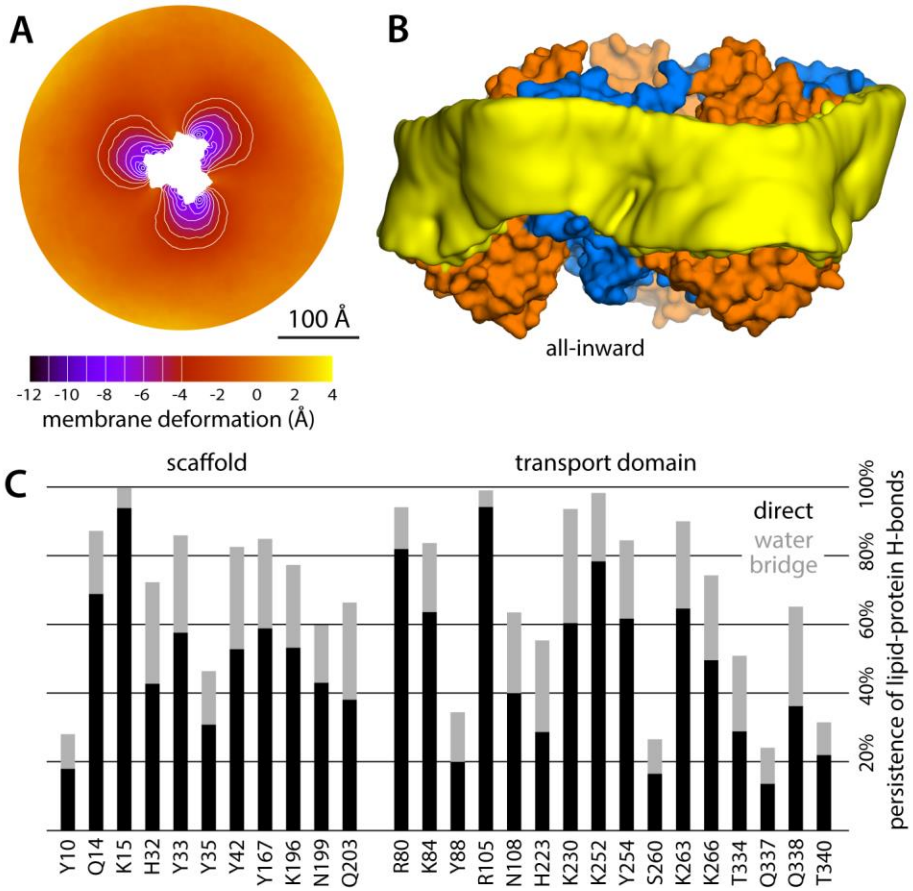

Figure 5. Membrane deformation induced by all-inward Glt_{Ph}, based on large-scale all-atom simulations in DPPC at 323 K. (**A**) Deflection of the membrane mid-plane relative to a flat surface, calculated exactly as in Fig. 2A. The standard error of the data (*N* = 3 trajectories, 150 ns each) across the deflection map is, on average, 1.5 Å. (**B**) Structure of all-inward Glt_{Ph} (as in Fig. 1), alongside a calculated density map for the lipid bilayer alkyl chains within 10 Å from the protein surface (yellow), based on all simulation data gathered for this state. See also Movie S3. (**C**) Hydrogen-bonding lipid-protein interactions observed during the all-atom simulations of all-inward Glt_{Ph}. Direct donor-acceptor interactions are considered, as are interactions mediated by a water molecule. For each protein side chain, the plot quantifies the fraction of the simulation time during which an interaction with a lipid was observed. Fig. 1C indicates the location of most of the side chains observed to have persistent lipid interactions.

Video 3. Membrane deformation induced by all-inward Glt_{Ph} in large-scale all-atom simulations. The structure of the protein is represented as in Fig. 1, and shown alongside a calculated density map for the lipid bilayer alkyl chains within 10 Å from the protein surface (yellow). The density map derives from three 150-ns simulations of a molecular system comprising over 3,000,000 atoms. The bilayer consists of DPPC lipids, at 323 K.

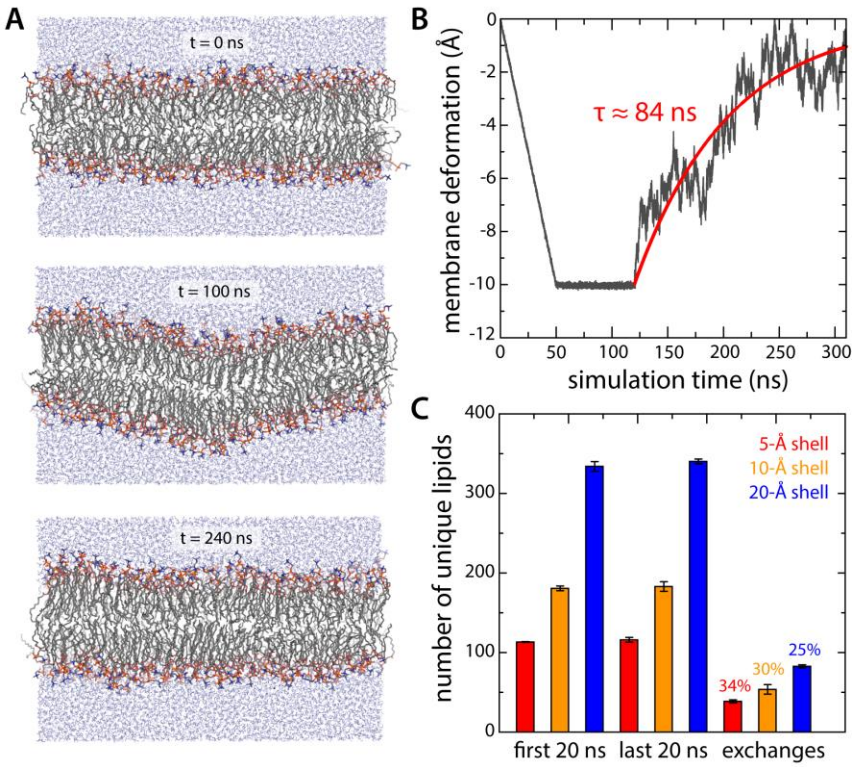

Figure 5 – figure supplement 1. Evaluation of potential biases resulting from conversion of coarse-grained molecular configurations into an all-atom representation. (**A, B**) All-atom simulation of the relaxation of an artificial 10-Å deflection in the membrane mid-plane. Given the large system size of the all-atom simulation system for all-inward Glt_{Ph} (~3,000,000 atoms), we sought to determine the minimum sampling time required to evaluate whether the membrane deformation induced by the protein in coarse-grained simulations was compatible with this more accurate representation. To this end we constructed a simulation system consisting of a 640-DPPC lipid bilayer (323 K) and ~32,700 TIP3P water molecules, enclosed in a periodic box of ~140 × 140 × 80 Å. After equilibration, an artificial deflection of the membrane mid-plane was created in this bilayer whose magnitude is comparable to that observed in the simulations of inward-facing Glt_{Ph} (see Fig. 2A). To create this perturbation, lipid molecules inside a cylinder of ~10 Å in radius were progressively displaced perpendicularly to the plane of the membrane by applying a harmonic restraint with a moving center and force constant of 100 kcal/mol $Å^{-2}$. The rate of movement of the restraint center was such that after 50 ns of simulation the vertical deflection was 10 Å; this value was then sustained for 70 ns, using the same restraint, now stationary. An unrestrained simulation of ~200 ns was carried out thereafter to evaluate the persistence or relaxation of the membrane deformation, during which we observed that the membrane relaxed fully within ~150 ns. Accordingly, each of the 3 all-atom trajectories calculated for inward-facing Glt_{Ph} was 150 ns long. (**C**) Lipid dynamics in the all-atom simulations of inward-facing Glt_{Ph}. The plot quantifies the number of lipid molecules that reside in three different shells around the protein (of 5, 10 or 20 Å width – red, orange and blue, respectively) for at least 50% of a 20-ns window at the beginning of the simulations (N = 3). The same values are given for a 20-ns window at the end of the simulations. The number of lipid molecules found in the latter set but not the former gives the number of exchanges between lipid molecules inside the shell and those further away from the protein.

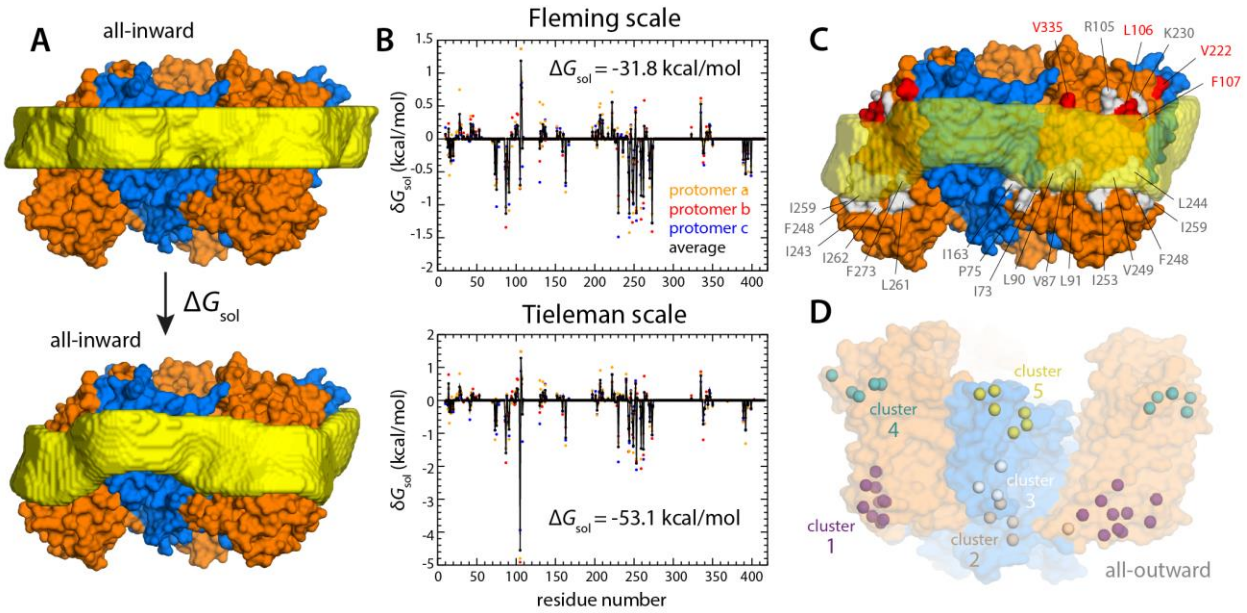

Figure 6. Energetics of solvation and evolutionary conservation of the Glt_{Ph} lipid interface. (**A**) Molecular systems used to evaluate the change in the free energy of polar/hydrophobic solvation that results from membrane bending, for all-inward Glt_{Ph}. The solvent-accessible surface area of each residue in the protein was calculated for either case (Methods). (**B**) Per-residue change in the free-energy of polar/hydrophobic solvation, deduced from two alternative hydrophobicity scales (Methods). Negative values of δG_{sol} indicate the deformed membrane state is favored; positive values favor the flat configuration instead. All residue contributions, in the 3 protomers, were summed to obtain the total value of ΔG_{sol}. (**C**) Residues for which the magnitude of δG_{sol} is 1 k_BT or greater (with both scales) are highlighted in the context of the proposed membrane deformation for all-inward Glt_{Ph}. Residues that favor the deformed state are shown in gray; those that favor the flat state are shown in red. The protein structure examined in panels (A, B) is an equilibrated snapshot of the all-atom simulation of all-inward Glt_{Ph}. An analogous analysis of the X-ray structure of all-inward Glt_{Ph} is shown in Fig. 6 – fig. suppl. 1. (**D**) Residues involved in H-bonds to lipid head groups (Fig. 5C) that are also predicted to have co-evolved with neighboring residues at the protein-lipid interface (Methods). The position of these residues in the outward-facing X-ray structure of Glt_{Ph} is indicated by their Cα atoms (spheres). On the cytoplasmic side of the protein, there are 3 main clusters: one on the transport domain (cluster 1, purple) comprising residues E80, K84 and Y88 (TM3), L250, Y254 (TM6), I411, V412, K414, T415, and E416 (TM12); and two mostly on the scaffold: one including A67 (TM3), A164, Y167 (TM4), K196, and G200 (TM5) (cluster 2, gray), and the other including K15 (TM1), Q203 and I207 (TM5) (cluster 3, white). On the periplasmic side, there are 2 clusters: one on the transport domain (cluster 4, cyan), comprising R105, N108 (TM3), F323 (TM7), V335, and Q338 (HP2a); and one on the scaffold (cluster 5, yellow) containing L30, H32, Y33 (TM1), T41, Y42, and V43 (TM2).

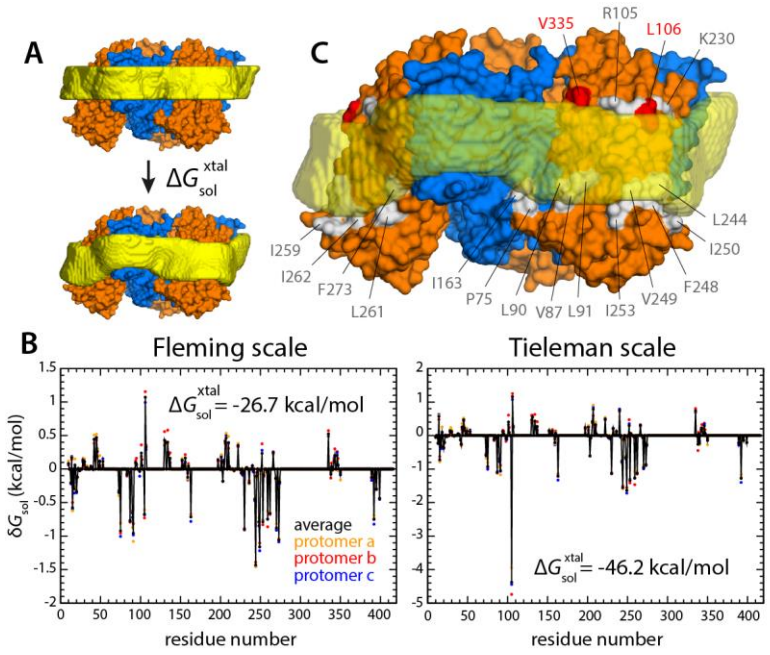

Figure 6 – figure supplement 1. Energetics of polar and hydrophobic solvation of the Glt_{Ph} lipid interface. Panels (A), (B) and (C) display information analogous to that shown in Fig. 6, but for the X-ray structure of all-inward Glt_{Ph} (PDB 3KBC).

The inward-facing state incurs a major energetic penalty due to membrane bending

The data presented in **Fig. 2-5** shows each Glt_{Ph} protomer causes a membrane deflection of about 10 Å in an area of about 1,000 $Å^2$, i.e., a very pronounced change in membrane curvature. This observation begs the question: what is the energetic cost of such a deformation? To answer this question precisely is very challenging. As we discuss in detail elsewhere (Fiorin, 2019), most computational strategies to examine the energetics of membrane bending are based upon the Helfrich-Canham theory, which predicts a relationship between curvature and energy dictated by the bending modulus of the bilayer (Canham, 1970; Helfrich, 1973). Although this theory is appropriate for mesoscopic perturbations, it can be inadequate on its own in the length scales that are relevant to membrane protein mechanistic studies (Goetz, 1999; Brannigan, 2006). Hence, a number of variations and extensions of the Helfrich-Canham function have been proposed to account for other possible contributions to the membrane energetics, based on more complex functions of the local bilayer curvature (Brannigan, 2006; Watson, 2012; Khelashvili, 2013). An alternative route to evaluate membrane perturbations would be to calculate the associated free-energy cost directly from a molecular dynamics simulation, using enhanced-sampling techniques. This type of model-free, microscopic approach has become state-of-the-art in computational studies of other molecular-scale processes such as ion permeation, ligand binding, or protein conformational change (Perez, 2016; Harpole, 2018; Flood, 2019), superseding other types of models and theories. The

reason why microscopic enhanced-sampling approaches have lagged behind for membranes is the difficulty in formulating appropriate descriptors of the membrane shape and configuration – i.e. the so-called 'collective variable' problem.

In a recent development, we have reported a novel free-energy simulation strategy to address this problem, which we refer to as Multi-Map (Fiorin, 2019). The central element of this method is a collective variable that quantifies the similarity between the instantaneous configuration of the lipid membrane and a set of pre-defined density distributions mapped onto a 3D grid. Biased exploration of this Multi-Map variable, for example using umbrella-sampling simulations, not only transforms the bilayer shape as dictated by the set of target density distributions, but also permits derivation of the corresponding potential-of-mean-force. What, then, is the free-energy cost of the membrane deformations induced by inward-facing Glt_{Ph}?

To evaluate this cost, we devised a Multi-Map calculation whereby a lipid membrane is driven to deform in a manner that mimics the perturbation caused by Glt_{Ph}, but in the absence of the protein. In **Fig. 7A**, we show 2D representations of three membrane configurations sampled by this enhanced-simulation methodology. The simulations also sample configurations for which the amplitude of the membrane perturbations is greater and smaller than those shown in **Fig. 7A**, i.e., larger and smaller values of the Multi-Map variable. The corresponding potential-of-mean-force curve, i.e., the free-energy change as a function of the deformation amplitude, is shown in **Fig. 7B**. From comparison of this data with the results shown in **Fig. 2A**, it can be inferred that the cost of the membrane perturbation induced by all-inward Glt_{Ph} is on the order of 20 kcal/mol in total, or 6-7 kcal/mol per protomer. (This value was obtained in the absence of membrane tension; under membrane tension, the cost would be greater, as shown in **Fig. 7B**, but the extent of the deformation is smaller, as shown in **Fig. 3.**) Clearly, this energetic penalty is sizable; as noted above, however, energetic gains that result from polar and hydrophobic solvation of the protein surface when the membrane is deformed are comparable in magnitude, if not greater (**Fig. 6**). At any rate, this analysis shows that the morphological preference of the membrane is a major contributor to the free-energy landscape of this transporter; it specifically and strongly opposes the inward-facing state, and so must be counterbalanced by other free-energy contributions for the transporter to carry out its structural mechanism. (For completeness, a comparative analysis with results obtained using the Helfrich-Canham macroscopic theory is presented and discussed in **Fig. 7 – fig. suppl 1.**)

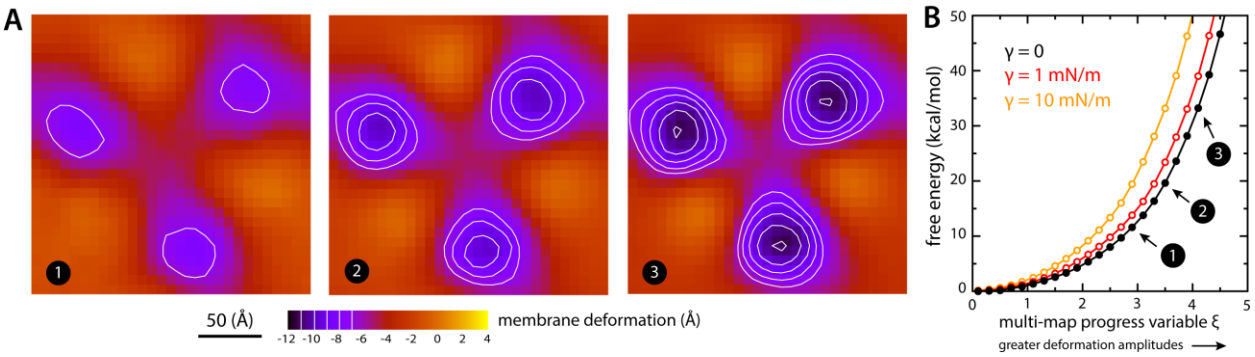

Figure 7. Estimate of the free-energy cost associated with the membrane deformation caused by all-inward Glt_{Ph}, from direct potential-of-mean-force calculations. (**A**) Simulated membrane deformation, in the absence of the protein, induced by application of the Multi-Map method in combination with umbrella-sampling, for a coarse-grained POPC lipid bilayer at 298 K. The figure shows three deflection maps analogous to those shown in Fig. 2A, i.e., calculated from trajectory data by averaging the *Z* coordinate of the bilayer mid-plane across the range of *X* and *Y* encompassed by the simulation box. The deflection maps shown correspond to three individual umbrella-sampling windows used in this free-energy calculation, differing in the amplitude of the perturbation that is induced in each case. Other trajectories/windows sample deformation amplitudes that are smaller or larger than those represented in the figure, i.e. smaller or larger values of the Multi-Map variable. Each map reflects an average of 18 independent simulations of 1 μs each. (**B**) Potential-of-mean-force (PMF) curve for the morphological perturbation depicted in panel (A), as a function of the Multi-Map variable, i.e., as a function of an increasing deformation amplitude. The free-energy values for the three configurations represented in panel (A) are indicated. PMF curves are also shown for two additional calculations based on umbrella-sampling simulations under an applied membrane tension, for the values indicated. Each of these PMF curves is an average of 18 independent calculations, each sampling 1 μs per window. Error bars for each curve average to about 0.6 kcal/mol.

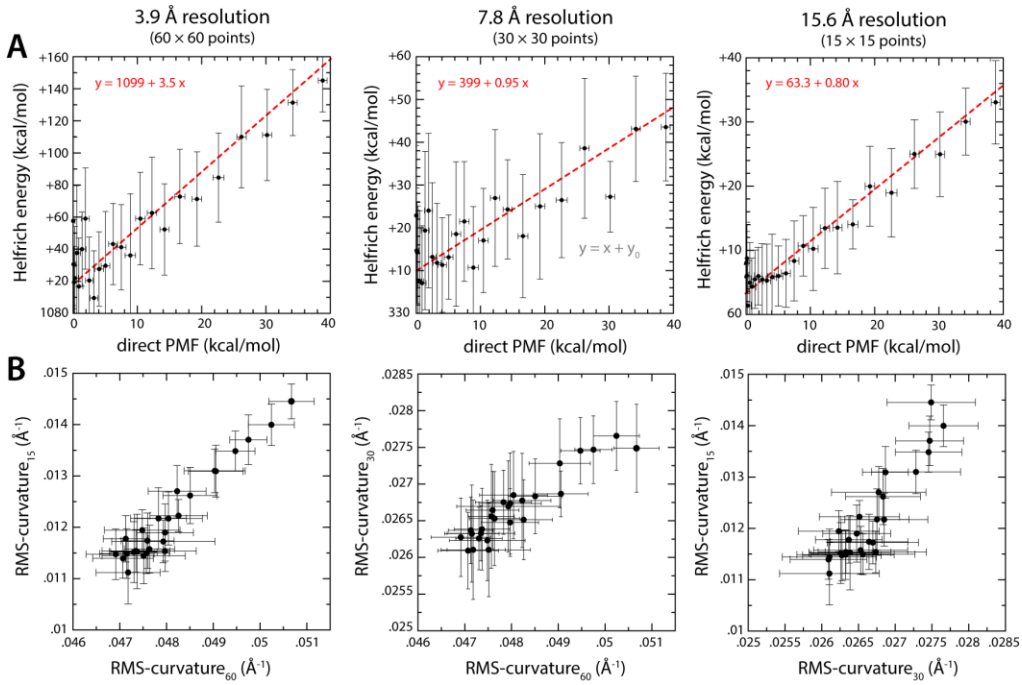

Figure 7 – figure supplement 1. Comparison of membrane-bending free-energy values calculated with the Multi-Map method and with the Helfrich-Canham theory, for the same ensembles of molecular configurations. (**A**) The PMF curves shown in Fig. 7 are correlated with energy profiles calculated with the Helfrich-Canham equation. Calculation of the latter requires two inputs: the assumed bending modulus k_c and the membrane curvature distribution across the *X*-*Y* plane, $c(x, y)$. For each of the umbrella-sampling windows used in the PMF calculation (18 trajectories × 1 μs), i.e., for each value of the progress variable ξ, we evaluate this curvature distribution from analysis of the average mid-plane of the membrane; specifically, maps such as those shown in Fig. 7A were interpolated with cubic splines and differentiated with respect to coordinates *x* and *y* to obtain the corresponding local curvature maps, $c(x, y)$. The elastic energy for each value of ξ was then calculated by integrating the Helfrich-Canham energy density $[0.5\ k_c\ c^2(x, y)]$ over the area of the membrane. The 3 plots in panel (A) describe Helfrich-Canham calculations that use the same value of k_c, namely 18 kcal/mol (Fiorin, 2019), but differ in the level of resolution used to quantify $c(x, y)$, as indicated. Linear regressions of the data in each case (using points up to ~100 kcal/mol – dashed red lines) show that the Helfrich-Canham energies can be much larger, similar or somewhat smaller that the PMF values depending on the resolution used for this curvature evaluation. (**B**) Comparison of curvature evaluations carried out at different resolutions. Specifically, for each umbrella-sampling window we compute the root-mean-squared curvature across the whole bilayer plane and contrast different resolutions. Despite extensive simulation time, i.e., 18 trajectories × 1 μs per window, the evaluation of the local membrane curvature is prone to large statistical errors (which propagate to the energy calculations) and ill-defined averages for moderate to low curvature values. By contrast, the PMFs curves shown in Fig. 7 approximately converge after 1 μs of sampling per window. In our view, these ambiguities in the definition of membrane curvature and the appropriate value of the bending modulus highlight the merits of direct PMF calculations such as those shown in Fig. 7.

Discussion

Our simulations predict that the conformational cycle of Glt_{Ph} induces a long-ranged remodeling of the surrounding lipid membrane, as a result of the elevator-like motion of the transport domains, each of which displaces its protein-lipid interface by about one-half the width of the bilayer hydrophobic core. Strikingly, this perturbation is abruptly suppressed at the point where the bilayer meets the trimerization domain; therefore, each protomer induces an independent deformation, consistent with existing experimental evidence demonstrating no protomer-protomer cooperativity in this class of transporters (Grewer, 2005; Koch, 2005; Koch, 2007; Leary, 2007; Akyuz, 2013; Erkens, 2013; Akyuz, 2015; Ruan, 2017). These results provide a working hypothesis and as such require experimental verification; while direct structural data confirming the drastic effects that we predict here are still lacking, such information is not beyond reach. As demonstrated by recent structural studies of Ca^{2+}-dependent lipid scramblases, single-particle cryo-EM can reveal the morphological features of detergent micelles and lipid nanodiscs in considerable detail (Falzone, 2018; Falzone, 2019; Kalienkova, 2019); crystallographic studies can also reveal the contours of the lipid bilayer, as observed for stacked membrane crystals of the SERCA Ca^{2+}-ATPase pump (Sonntag, 2011). Analogous data for alternate conformational states of Glt_{Ph}, or a close homolog thereof, ought to validate or refute the predicted impact of this transporter on the membrane morphology.

Single-molecule FRET measurements of substrate-loaded and substrate-free Glt_{Ph} in outside-out proteoliposomes have indicated that the intrinsic free-energy difference between the outward- and inward-facing states of the transporter is approximately zero, i.e., both states are approximately equally populated (Akyuz, 2013; Erkens, 2013; Akyuz, 2015). Here, we have shown that the membrane deflection induced by inward-facing Glt_{Ph} translates into a substantial energetic penalty, which we believe to be in the order of 6-7 kcal/mol per protomer, or about 20 kcal/mol in total. To balance out this cost, therefore, the inward-facing conformation must somehow recoup this energy, through distinct protein-protein, protein-lipid and/or protein-water interactions. Admittedly, at this point we can only infer the magnitude of the free-energy penalty, from simulations where the Multi-Map method mimics the impact of the protein on the membrane. While imperfect, it is worth underscoring the technical breakthrough made by this approach: it provides a means to estimate the membrane energetics directly from simulated molecular-dynamics trajectories, without a priori theoretical assumptions. Thus, we believe that further methodological developments and systematic applications of this methodology, in combination with other enhanced-sampling techniques, will result in increasingly precise estimates, and will also enable us to dissect the compensating interactions that must occur in this and other membrane-protein systems. These caveats notwithstanding, we believe our estimate of the free-energy penalty of membrane bending not to be at all unrealistic. For example, based on electrophysiological studies of the gating mechanism of the *Shaker* voltage-gated K^+ channel, it has been deduced that at zero membrane potential the conformational free-energy of the open state is about 15 kcal/mol lower than that of the closed state (Chowdhury, 2012). Similarly, a value of 16 kcal/mol was deduced for the Na^+-channel $Na_v1.4$ (Chowdhury, 2012). Regardless of the specifics, this study underscores that the configurational energetics of the lipid bilayer are non-negligible and must therefore be incorporated into the conceptual models and theories used to describe membrane-protein

mechanisms – much in the same way one would consider, for example, the dehydration energetics of different ions (also in the order of tens of kcal/mol) when rationalizing the selectivity or conductance rates of a channel protein. It is hoped, therefore, that the calculations presented here will spur further biophysical studies designed to assess the impact of bilayer composition and morphology on the energetics of transporters – in analogy with research in other membrane proteins such as receptors (Brown, 2017) and channels (Phillips, 2009; Andersen, 2013). For example, it would be of interest to dissect how the functional dynamics of a transporter such as Glt_{Ph} are influenced by the amino-acid make-up of the protein-lipid interface, as well as by lipid bilayer composition. Indeed, functional studies have shown that subtle lipid modifications (methylation) and single-point mutations (Tyr33) have detectable effects on the rates of Glt_{Ph} transport (McIlwain, 2015). It is also intriguing that long-chain polyunsaturated fatty acids (PUFA) modulate the activity of neuronal EAAT transporters (Zerangue, 1995; Fairman, 1998; Tzingounis, 1998; Grintal, 2009) and are also known to influence the bending energetics of lipid bilayers (Cordero-Morales, 2018).

The aforementioned smFRET studies have also indicated that the balance of outward- and inward-facing states hardly differs when measured in liposomes (containing mostly PE, PG and PC lipids) or in DDM micelles (Akyuz, 2015). Taken together with our findings, this observation challenges the notion that detergent micelles have no distinct morphological preference and will comply to the conformation of a protein at little or no energetic cost. To the contrary, when a detergent solution is concentrated above a certain threshold, the micelles that form have an inherently preferred geometry and size (Lipfert, 2007; Oliver, 2013), i.e., there exists a well-defined free-energy minimum of micelle formation. When a micelle assembles around a protein, one might expect that free-energy minimum to naturally shift, i.e., the micelle morphology will adapt to the volume and surface of the protein. However, this adaption is not necessarily identical for all conformations of a protein; indeed, one might expect that different free-energy minima will exist for alternative structural states (both in magnitude and morphology), and that this difference in will be greater for some detergents than for others. The expectation that the deformation of a micelle entails little or no energetic cost is even less intuitive if one assumes that the micelle does not reassemble when a protein changes structure. Indeed, the above-mentioned cryo-EM data for nhTMEM16 shows that a highly localized feature of the protein surface causes nearly identical morphological changes in a lipid nanodisc and in a DDM micelle, namely a slowly-changing perturbation that gradually decays along the protein perimeter (Kalienkova, 2019). If the DDM micelle was indeed much softer or more compliant than the lipid nanodisc, the resulting curvature would be more localized. Thus, on this matter too we believe our data highlights the need for further work probing how the thermodynamics of micellar or lipid solvation might depend on the conformational state of a protein, or on its oligomerization state.

The dynamics of Glt_{Ph} at the single-molecule level have also been evaluated using high-speed AFM measurements in protein-dense 2D preparations (Ruan, 2017). These elegant measurements clearly confirmed that each protomer exchanges between outward- and inward-facing states stochastically (provided the adequate occupancy state) and independently from each other. Intriguingly, though, in these measurements the population ratio between outward- and inward-facing is shifted significantly against the latter, by about 5-fold (Ruan,

2017; Heath, 2019). A possible explanation for the discrepancy between the smFRET and AFM measurements is that the curvature of the outside-out proteoliposomes used in the former experiment favors the inward-facing state, while the flat membranes in the latter do not. However, our finding that the membrane perturbation caused by Glt_{Ph} projects away from the protein surface for several nanometers provides an alternative explanation: transition to the inward-facing state would be more energetically costly when this deformation must occur in a more confined space. In other words, it is conceivable that the aforementioned balance between large, competing energetic contributions is altered as a result of molecular crowding, in this case favoring the outward-facing conformation. Interestingly, some members of the EAAT family are expressed in the membranes of certain cell types at very high densities (in the order of thousands of transporters per square-micron (Danbolt, 2001)), raising the possibility that crowding effects occur in physiological settings. On a related, more technical note, it is worth noting that molecular simulation studies aiming to evaluate the alternating-access mechanism and protein-lipid interplay for cases such as Glt_{Ph} might be significantly skewed by finite-size effects if the lipid bilayer patch is not sufficiently large to accommodate the full range of the membrane perturbation created by the protein.

Large-scale structural changes are not exclusive to membrane proteins in the EAAT superfamily. Elevator-like secondary-active transporters are, however, appealing model systems to evaluate the interplay between proteins and the lipid bilayer, given the range of their motions and that these motions occur spontaneously and, in some cases, on time-scales amenable to single-molecule measurements like smFRET or high-speed AFM. As an example of another elevator-like mechanism, an initial analysis of the bacterial sodium-dicarboxylate symporter VcINDY is shown in **Fig. 8**. VcINDY is a dimer, but is similar to Glt_{Ph} in that each of the constituent protomers features two distinct domains, one facilitating dimerization and the other responsible for substrate translocation (Mancusso, 2012; Mulligan, 2016). Our simulations show that upon transition to the (predicted) inward-facing state, the transport domains would induce a deformation in the membrane that is comparable to that observed for Glt_{Ph}. Again, this deformation is suppressed by the scaffold, suggesting that the protomers function independently. Despite the commonalities between Glt_{Ph} and VcINDY, however, it is important to note that other elevator-like transporters, perhaps even those in the same structural family, might influence the membrane differently, as this interplay is ultimately determined by the amino-acid make-up of the protein surface. For example, it is entirely possible that, in some cases, the outward-facing state perturbs the membrane the most. To document and dissect this variability is no doubt of interest and will be the focus of future studies.

Glt_{Ph} and VcINDY are stark examples of membrane proteins that cause large-scale morphological changes in the bilayer. Needless to say, numerous channels and transporters also undergo major conformational changes during function, which might impact the membrane to varying degrees. The computational analysis presented here makes it clear that the inherent configurational energetics of the lipid bilayer can be both non-negligible and markedly state-dependent, and must therefore be integrated in our conceptualizations of membrane protein mechanisms.

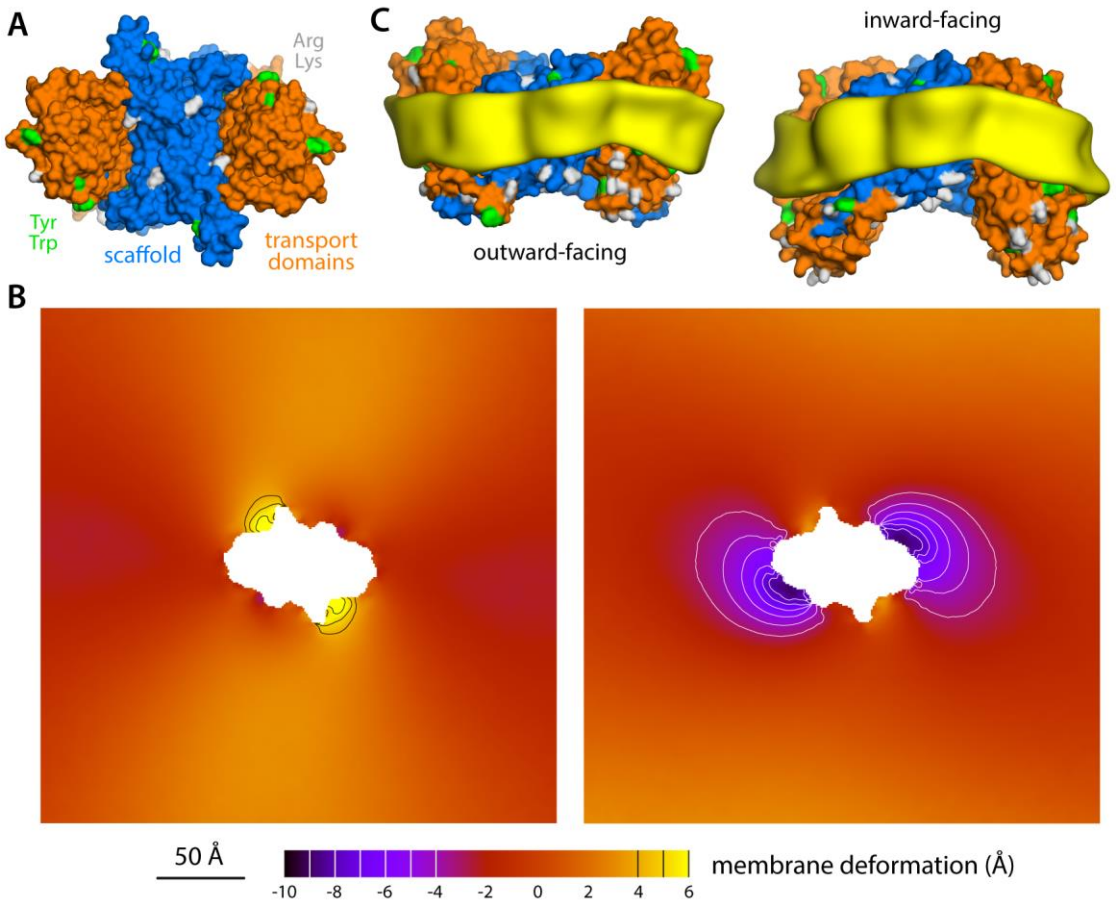

Figure 8. Membrane deformation induced by the Na^+-dicarboxylate symporter VcINDY, based on coarse-grained MD simulations in POPC at 298 K. (**A**) Experimental crystal structure of the VcINDY dimer in the outward-facing state, viewed along the membrane perpendicular from the extracellular space. The protein is represented as Glt_{Ph} in Fig. 1. (**B**) Deflection of the membrane mid-plane induced by VcINDY in the outward- and inward-facing states (left and right, respectively) based on three independent simulations for either state. The view is from the extracellular space. From left to right, the standard error of the data (N = 3) across each map is, on average, 1.0 Å and 0.8 Å. (**C**) Structures of outward- and inward-facing VcINDY (represented as in panel A), alongside calculated density maps for lipid alkyl chains within 10 Å from the protein surface (yellow), based on all the simulation data obtained for either state. Note the structure of inward-facing state is a model, constructed on the basis of the outward-facing conformation through repeat-swapping (Mulligan, 2016).

Methods

Coarse-grained simulations of Glt_{Ph} trimers and VcINDY dimers

Four different conformational states of the Glt_{Ph} transporter were simulated using a coarse-grained (CG) representation of the protein and its environment, using the MARTINI 2.1 forcefield (Marrink, 2007). Symmetric trimers of outward- and inward-facing conformers were obtained from X-ray crystal structures (PDB 2NWL and 3KBC, respectively (Boudker, 2007; Reyes, 2009)). These differ primarily in the position of the transport domains (defined here as residues 74-129 and 223-416), relative to the central oligomerization domain, or scaffold (residues 6-73 and 120-222). Two asymmetric trimers were also considered, combining two outward- and one inward-facing protomer, or two inward- and one outward-facing protomer. These intermediates were constructed by superposing the scaffold domain of individual protomers from the inward-facing structure onto the trimer with all protomers outward-facing. All four states of the transporter were embedded in a hydrated bilayer of 1-palmitoyl-2-oleoyl-sn-glycero-3-phosphocholine (POPC) lipids, to evaluate the morphological adaption of the membrane to the protein conformation. The conformation of each state was maintained throughout the simulations by applying a network of harmonic distance restraints to a pre-defined set of pairs of non-bonded protein atoms. This set comprises all pairs of backbone atoms separated by a distance between 5 and 9 Å; the force constant of these elastic restraints is 1.2 kcal/mol $Å^{-2}$. The protein-membrane systems include ~7,500 lipids and ~170,000 solvent molecules, for a total of ~260,000 particles. The dimensions of the simulation systems are approximately 500 × 500 × 120 Å.

All CG simulations were carried out using GROMACS 4.5.5 (Hess, 2008), with a 10-fs integration time-step. Temperature and pressure were maintained constant using the Berendsen barostat and thermostat (Berendsen, 1984). The pressure (1 atm) was applied semi-isotropically, i.e. *X* and *Y* dimensions (the bilayer plane) fluctuate but at constant *X*/*Y* ratio, while fluctuations in *Z* are independent. Unless specified otherwise, the pressure components P_{XX}, P_{YY} and P_{zz} were such that the resulting membrane tension is zero. Periodic boundary conditions were used. Non-bonded interactions were described by a shifted Lennard-Jones potential, cut-off at 12 Å, and by a Coulombic potential with relative dielectric constant $\varepsilon_r = 15$.

For each Glt_{Ph} state, we calculated 3 independent trajectories of 600 ns. Analogous, triplicated simulations of 600 ns were also carried out for all-inward Glt_{Ph} in a bilayer of 1,2-dipalmitoyl-sn-glycero-3-phosphocholine (DPPC) lipids at 323 K; in a mixed bilayer of 1-palmitoyl-2-oleoyl-sn-glycero-3-phosphoethanolamine (POPE) lipids and 1-palmitoyl-2-oleoyl-sn-glycero-3-phospho-(1'-rac-glycerol) (POPG) lipids in a 2:1 ratio, at 298K; and in a bilayer of POPE lipids, also at 298 K. Triplicated simulations of 600 ns were also carried out for all-inward Glt_{Ph} in POPC at 298 K under applied membrane tensions of 1, 5 and 10 mN/m. Finally, triplicated simulations of 600 ns each were carried out for the Na^+-dicarboxylate transporter VcINDY, in POPC at 298 K, in both outward- and inward-facing conformations; the former corresponds to the experimentally determined X-ray structure (PDB 5ULD (Mancusso, 2012)) while the latter is a computational model (Mulligan, 2016).

All-atom simulations in all-inward Glt_{Ph}

For the all-inward state (with all three Glt_{Ph} protomers inward-facing) we also calculated 3 independent trajectories of 150 ns each, using an all-atom representation of the molecular system. The starting coordinates for each of these simulations were obtained from selected snapshots of the three independent CG simulations carried out for the all-inward state in DPPC. Specifically, we chose those snapshots in which the instantaneous shape of the membrane mid-plane showed the lowest RMS deviation from shape calculated by averaging all trajectory data for this all-inward state. Using an all-atom model of the protein derived from the crystal structure (PDB 3KBC), the surrounding (coarse-grained) membrane and solvent were transformed into an all-atom representation as prescribed elsewhere (Wassenaar, 2014), and equilibrated through a series of simulations implementing positional restraints. The final models comprise ~3,000,000 atoms. The all-atom simulations were carried out using NAMD version 2.9 (Phillips, 2005). The CHARMM36 force field (Klauda, 2010; Best, 2012) was used for the protein and the lipids, while the TIP3P model was adopted for the water (Jorgensen, 1983). To preserve the conformation of the protein, a restraint was applied to the RMSD of the C_α trace, relative to the experimental structure, of force constant 100 kcal/mol $Å^{-2}$. The simulations were carried out at constant temperature (323 K), using a Langevin thermostat, and constant semi-isotropic pressure (1 atm), using the Nose-Hoover Langevin barostat, with periodic boundaries. The integration time-step was 2 fs. Electrostatic interactions were calculated using Particle-Mesh Ewald with a real space cut-off of 12 Å. The same cut-off was also used for the shifted Lennard-Jones potential describing van der Waals interactions.

Energetics of polar/hydrophobic solvation

The molecular systems depicted in **Fig. 6A** show two membrane states: one deformed, and identical to that observed in our simulations (Fig. 5A), and a hypothetical version thereof with the same thickness (16 Å) but flat; both membranes are aligned at the scaffold. (In this context, 'membrane' refers to the solvent-excluded region of the bilayer). For each of these two systems, we calculated the solvent-accessible surface area (SASA) for each of the protein residues i, denoted by $A_{bent}(i)$ and $A_{flat}(i)$, using PyMol (Schrödinger, Inc) and a probe radius of 1.4 Å. A SASA value denoted as A_{max} (i) was also calculated for each amino-acid type when fully solvent-exposed in a GXG tri-peptide. The per-residue change in the free-energy of polar/ hydrophobic solvation (**Fig. 6B**) was then calculated as $\delta G_{sol}(i) = S_{transfer}(i) \times [\, A_{flat}(i) - A_{bent}(i) \,] / A_W(i)$, where $S_{transfer}(i)$ are identical for residues of the same type, and derive from two independent hydrophobicity scales: one based on experimental measurements of the stability of wild-type and mutagenized OMPLA, referred to as the Fleming scale (Moon, 2011); and another based on PMF calculations of side-chain analog insertion in a DOPC bilayer, referred to as the Tieleman scale (MacCallum, 2007). For His, Gly and Pro, which lack values in the latter scale, values from the Fleming scale were used in both calculations.

Coevolutionary analysis

The Uniprot sequence GLT_PYRHO was used as input to the EVcouplings server (Marks, 2011) with default parameters. The results can be considered to be robust because the ratio of effective sequences in the alignment (9,565 sequences obtained using a bit-score threshold of 0.3) to the length of the protein sequence is >20. To limit our search to reliable scores, we focused on pairs whose scores have coupling probabilities greater than 0.5, i.e., the top 0.8% of all possible pairs. To identify positions that co-evolved in order to maintain interactions with the lipid head groups, we focused on pairs involving at least one residue known to H-bond with lipids in the all-atom simulations of Glt_{Ph} (Fig. 5C). Pairs were excluded if they contained buried residues, or residues exposed only to the central aqueous vestibule, or were less than 8 residues apart in sequence, i.e., within two turns of a helix. The remaining pairs were assigned to a cluster if at least one residue was involved in more than one pair in that cluster.

Potential-of-mean-force (PMF) calculations

The recently developed Multi-Map method (Fiorin, 2019) was used to compute the free-energy cost of a membrane deformation that is similar to that induced by all-inward Glt_{Ph}, but in the absence of the protein. To this end, a set of 10 three-dimensional density maps that idealize this deformation but vary in its amplitude were generated and used to define the so-called Multi-Map coordinate ξ. This variable quantifies the similarity between any instantaneous configuration of the membrane and each of the density maps in the target set. Biased-sampling of the Multi-Map coordinate ξ thus perturbs the membrane as dictated by the set of target maps and permits a derivation of the corresponding free-energy cost as a function of the deformation amplitude, i.e. the potential of mean force (Fiorin, 2019). This technique was applied to a CG bilayer of 1,800 POPC molecules (L = 234 Å), using a developmental version of NAMD (Phillips, 2005) and analogous pressure and temperature conditions as those specified above. Umbrella-sampling was employed as the biasing method; the target range in ξ was divided into 61 windows, and 18 simulations of 1 μs each were carried out to sample ξ in each window. The PMF was calculated on the basis of the resulting time-series of ξ, using the WHAM method (Kumar, 1992). To examine the effect of membrane tension, analogous umbrella-sampling simulations and PMF curves were calculated under applied tensions of 1 and 10 mN/m.

Acknowledgements

The authors are grateful to numerous colleagues and lab members for their commentary on different aspects of this work – too numerous to be listed here. Special thanks are owed to Janice L. Robertson for useful discussions, and to Michael Grabe and co-workers for helping us to apply their continuum-mechanics method to examine the membrane deformations caused by elevator-like transporters. This research was initially supported by the Max Planck Society and The German Research Foundation, and subsequently by the Divisions of Intramural Research of the National Institute of Neurological Disorders and Stroke and of the National Heart, Lung and Blood Institute, National Institutes of Health (NIH). In part, this work utilized the computational resources of the NIH HPC facility Biowulf.

766

References

Akyuz, N., R. B. Altman, S. C. Blanchard and O. Boudker (2013). "Transport dynamics in a glutamate transporter homologue." Nature **502**(7469): 114.

Akyuz, N., E. R. Georgieva, Z. Zhou, S. Stolzenberg, M. A. Cuendet, G. Khelashvili, R. B. Altman, D. S. Terry, J. H. Freed, H. Weinstein, O. Boudker and S. C. Blanchard (2015). "Transport domain unlocking sets the uptake rate of an aspartate transporter." Nature **518**(7537): 68 73.

Andersen, O. S. (2013). "Membrane proteins: Through thick and thin." Nature Chemical Biology **9**(11): 667.

Andersen, O. S. and R. E. Koeppe (2007). "Bilayer Thickness and Membrane Protein Function: An Energetic Perspective." Biophysics and Biomolecular Structure **36**(1): 107-130.

Argudo, D., N. P. Bethel, F. V. Marcoline, C. W. Wolgemuth and M. Grabe (2017). "New Continuum Approaches for Determining Protein-Induced Membrane Deformations." Biophysical Journal **112**(10): 2159 2172.

Berendsen, H. J. C., J. P. M. Postma, W. F. van Gunsteren, A. DiNola and J. R. Haak (1984). "Molecular dynamics with coupling to an external bath." J. Chem. Phys. **81**: 3684-3690.

Best, R. B., X. Zhu, J. Shim, P. E. M. Lopes, J. Mittal, M. Feig and A. D. M. Jr (2012). "Optimization of the additive CHARMM all-atom protein force field targeting improved sampling of the backbone ϕ, ψ and side-chain χ(1) and χ(2) dihedral angles." Journal of Chemical Theory and Computation **8**(9): 3257 3273.

Bethel, N. P. and M. Grabe (2016). "Atomistic insight into lipid translocation by a TMEM16 scramblase." Proceedings of the National Academy of Sciences of the United States of America **113**(49): 14049 14054.

Boudker, O., R. M. Ryan, D. Yernool, K. Shimamoto and E. Gouaux (2007). "Coupling substrate and ion binding to extracellular gate of a sodium-dependent aspartate transporter." Nature **445**(7126): 387-393.

Boudker, O. and G. Verdon (2010). "Structural perspectives on secondary active transporters." Trends Pharm Sci **31**(9): 418-426.

Brannigan, G. and F. L. Brown (2006). "A consistent model for thermal fluctuations and protein-induced deformations in lipid bilayers." Biophys J. **90**(5): 1501-1520.

Brown, M. F., U. Chawla and S. M. D. C. Perera (2017). "The Biophysics of Cell Membranes, Biological Consequences." 61-84.

Canham, P. B. (1970). "Minimum energy of bending as a possible explanation of biconcave shape of human red blood cell." J. Theor. Biol. **26**(1): 61-&.

Chowdhury, S. and B. Chanda (2012). "Estimating the voltage-dependent free energy change of ion channels using the median voltage for activation." The Journal of General Physiology **139**(1): 3-17.

Cordero-Morales, J. F. and V. Vásquez (2018). "How lipids contribute to ion channel function, a fat perspective on direct and indirect interactions." Current Opinion in Structural Biology **51**(Nat Rev Mol Cell Biol 1842 2018): 92-98.

Corradi, V., E. Mendez-Villuendas, H. I. Ingólfsson, R.-X. Gu, I. Siuda, M. N. Melo, A. Moussatova, L. J. DeGagné, B. I. Sejdiu, G. Singh, T. A. Wassenaar, K. D. Magnero, S. J. Marrink and D. P.

Tieleman (2018). "Lipid–Protein Interactions Are Unique Fingerprints for Membrane Proteins." ACS Central Science **4**(6): 709-717.
Cui, Q., L. Zhang, Z. Wu and A. Yethiraj (2013). "Generation and sensing of membrane curvature: Where materials science and biophysics meet." Current Opinion in Solid State and Materials Science **17**(4): 164-174.
Danbolt, N. C. (2001). "Glutamate uptake." Progress in Neurobiology **65**(1): 1-105.
Denning, E. J. and O. Beckstein (2013). "Influence of lipids on protein-mediated transmembrane transport." Chemistry and Physics of Lipids **169**: 57-71.
Erkens, G. B., I. Hänelt, J. M. H. Goudsmits, D. J. Slotboom and A. M. v. Oijen (2013). "Unsynchronised subunit motion in single trimeric sodium-coupled aspartate transporters." Nature **502**(7469): 119.
Fairman, W. A., M. S. Sonders, G. H. Murdoch and S. G. Amara (1998). "Arachidonic acid elicits a substrate-gated proton current associated with the glutamate transporter EAAT4." Nature Neuroscience **1**(2): 105 113.
Falzone, M. E., J. Rheinberger, B.-C. Lee, T. Peyear, L. Sasset, A. Raczkowski, E. Eng, A. D. Lorenzo, O. S. Andersen, C. M. Nimigean and A. Accardi (2018). "Cryo-EM structures reveal bilayer remodeling during Ca2+ activation of a TMEM16 scramblase." bioRxiv: 420174.
Falzone, M. E., J. Rheinberger, B.-C. Lee, T. Peyear, L. Sasset, A. M. Raczkowski, E. T. Eng, A. D. Lorenzo, O. S. Andersen, C. M. Nimigean and A. Accardi (2019). "Structural basis of Ca2+-dependent activation and lipid transport by a TMEM16 scramblase." eLife **8**: e43229.
Fiorin, G., F. Marinelli and J. D. Faraldo-Gomez (2019). "Direct Derivation of Free Energies of Membrane Deformation and Other Solvent Density Variations From Enhanced Sampling Molecular Dynamics." J Comput Chem.
Flood, E., C. Boiteux, B. Lev, I. Vorobyov and T. W. Allen (2019). "Atomistic Simulations of Membrane Ion Channel Conduction, Gating, and Modulation." Chem Rev **119**(13): 7737-7832.
Forrest, L. R., R. Kraemer and C. Ziegler (2011). "The structural basis of secondary active transport mechanisms." Biochim. Biophys. Acta **1807**: 167-188.
Georgieva, E. R., P. P. Borbat, C. Ginter, J. H. Freed and O. Boudker (2013). "Conformational ensemble of the sodium-coupled aspartate transporter." Nature Structural & Molecular Biology **20**(2): 215.
Gether, U., P. H. Andersen, O. M. Larsson and A. Schousboe (2006). "Neurotransmitter transporters: molecular function of important drug targets." Trends in Pharmacological Sciences **27**(7): 375-383.
Goetz, R., G. Gompper and R. Lipowsky (1999). "Mobility and Elasticity of Self-Assembled Membranes." Physical Review Letters **82**(1): 221-224.
Grewer, C., P. Balani, C. Weidenfeller, T. Bartusel, Z. Tao and T. Rauen (2005). "Individual subunits of the glutamate transporter EAAC1 homotrimer function independently of each other." Biochemistry **44**(35): 11913-11923.
Grintal, B., G. Champeil-Potokar, M. Lavialle, S. Vancassel, S. Breton and I. Denis (2009). "Inhibition of astroglial glutamate transport by polyunsaturated fatty acids: Evidence for a signalling role of docosahexaenoic acid." Neurochemistry International **54**(8): 535-543.
Groeneveld, M. and D.-J. Slotboom (2007). "Rigidity of the subunit interfaces of the trimeric glutamate transporter GltT during translocation." J Mol Biol **372**(3): 565-570.

Hänelt, I., D. Wunnicke, E. Bordignon, H.-J. Steinhoff and D. J. Slotboom (2013). "Conformational heterogeneity of the aspartate transporter GltPh." Nature Structural & Molecular Biology **20**(2): 210.

Harpole, T. J. and L. Delemotte (2018). "Conformational landscapes of membrane proteins delineated by enhanced sampling molecular dynamics simulations." Biochim Biophys Acta Biomembr **1860**(4): 909-926.

Haselwandter, C. A. and R. MacKinnon (2018). "Piezo's membrane footprint and its contribution to mechanosensitivity." Elife **7**.

Heath, G. R. and S. Scheuring (2019). "Advances in high-speed atomic force microscopy (HS-AFM) reveal dynamics of transmembrane channels and transporters." Current Opinion in Structural Biology **57**(J Struct Biol 180 2012): 93-102-102.

Helfrich, W. (1973). "Elastic properties of lipid bilayers - theory and possible experiments." Z. Naturforsch. C **28**(11-1): 693-703.

Hess, B., C. Kutzner, D. van der Spoel and E. Lindahl (2008). "GROMACS 4: Algorithms for Highly Efficient, Load-Balanced, and Scalable Molecular Simulation." J. Chem. Theory Comput. **4**(3): 435-447.

Jardetzky, O. (1966). "Simple allosteric model for membrane pumps." Nature **211**(5052): 969-970.

Javanainen, M., H. Martinez-Seara and I. Vattulainen (2017). "Excessive aggregation of membrane proteins in the Martini model." PLoS ONE **12**(11): e0187936.

Jensen, M. Ø. and O. G. Mouritsen (2004). "Lipids do influence protein function—the hydrophobic matching hypothesis revisited." Biochimica et Biophysica Acta (BBA) - Biomembranes **1666**(1-2): 205-226.

Jorgensen, W. L., J. Chandrasekhar, J. D. Madura, R. W. Impey and M. L. Klein (1983). "Comparison of simple potential functions for simulating liquid water." The Journal of Chemical Physics **79**(2): 926 935.

Kalienkova, V., V. C. Mosina, L. Bryner, G. T. Oostergetel, R. Dutzler and C. Paulino (2019). "Stepwise activation mechanism of the scramblase nhTMEM16 revealed by cryo-EM." eLife **8**: e44364.

Khelashvili, G., B. Kollmitzer, P. Heftberger, G. Pabst and D. Harries (2013). "Calculating the bending modulus for multicomponent lipid membranes in different thermodynamic phases." J. Chem. Theory Comput. **9**(9): 3866-3871.

Klauda, J. B., R. M. Venable, J. A. Freites, J. W. O'Connor, D. J. Tobias, C. Mondragon-Ramirez, I. Vorobyov, A. D. M. Jr and R. W. Pastor (2010). "Update of the CHARMM all-atom additive force field for lipids: validation on six lipid types." The Journal of Physical Chemistry B **114**(23): 7830 7843.

Koch, H. P., R. L. Brown and H. P. Larsson (2007). "The glutamate-activated anion conductance in excitatory amino acid transporters is gated independently by the individual subunits." Journal of Neuroscience **27**(11): 2943-2947.

Koch, H. P. and H. P. Larsson (2005). "Small-scale molecular motions accomplish glutamate uptake in human glutamate transporters." J. Neurosci. **25**(7): 1730-1736.

Kumar, S., J. M. Rosenberg, D. Bouzida, R. H. Swendsen and P. A. Kollman (1992). "THE weighted histogram analysis method for free-energy calculations on biomolecules. I. The method." Journal of Computational Chemistry **13**(8): 1011-1021.

Leary, G. P., E. F. Stone, D. C. Holley and M. P. Kavanaugh (2007). "The glutamate and chloride permeation pathways are colocalized in individual neuronal glutamate transporter subunits." Journal of Neuroscience **27**(11): 2938-2942.
Lee, A. G. (2004). "How lipids affect the activities of integral membrane proteins." Biochimica et Biophysica Acta (BBA) - Biomembranes **1666**(1-2): 62-87.
Lee, K., II, R. W. Pastor, O. S. Andersen and W. Im (2013). "Assessing smectic liquid-crystal continuum models for elastic bilayer deformations." Chemistry and Physics of Lipids **169**: 19-26.
Lipfert, J., L. Columbus, V. B. Chu, S. A. Lesley and S. Doniach (2007). "Size and Shape of Detergent Micelles Determined by Small-Angle X-ray Scattering." The Journal of Physical Chemistry B **111**(43): 12427-12438.
MacCallum, J. L., W. F. Bennett and D. P. Tieleman (2007). "Partitioning of amino acid side chains into lipid bilayers: results from computer simulations and comparison to experiment." J Gen Physiol **129**(5): 371-377.
Mancusso, R., G. G. Gregorio, Q. Liu and D.-N. Wang (2012). "Structure and mechanism of a bacterial sodium-dependent dicarboxylate transporter." Nature **491**: 622.
Marks, D. S., L. J. Colwell, R. Sheridan, T. A. Hopf, A. Pagnani, R. Zecchina and C. Sander (2011). "Protein 3D structure computed from evolutionary sequence variation." PLoS One **6**(12): e28766.
Marrink, S.-J., H. J. Risselada, S. Yefimov, D. P. Tieleman and A. H. d. Vries (2007). "The MARTINI Force Field: Coarse Grained Model for Biomolecular Simulations." The Journal of Physical Chemistry B **111**(27): 7812 7824.
Marrink, S. J., V. Corradi, P. C. T. Souza, H. I. Ingólfsson, D. P. Tieleman and M. S. P. Sansom (2019). "Computational Modeling of Realistic Cell Membranes." Chemical Reviews **119**(9): 6184-6226.
Marrink, S. J., A. H. d. Vries and A. E. Mark (2004). "Coarse Grained Model for Semiquantitative Lipid Simulations." The Journal of Physical Chemistry B **108**(2): 750-760.
Marsh, D. (2008). "Protein modulation of lipids, and vice-versa, in membranes." Biochimica et Biophysica Acta (BBA) - Biomembranes **1778**(7-8): 1545-1575.
McIlwain, B. C., R. J. Vandenberg and R. M. Ryan (2015). "Transport rates of a glutamate transporter homologue are influenced by the lipid bilayer." Journal of Biological Chemistry **290**(15): 9780 9788.
Mondal, S., G. Khelashvili, J. Shan, Olaf S. Andersen and H. Weinstein (2011). "Quantitative Modeling of Membrane Deformations by Multihelical Membrane Proteins: Application to G-Protein Coupled Receptors." Biophysical Journal **101**(9): 2092-2101.
Monticelli, L., S. K. Kandasamy, X. Periole, R. G. Larson, D. P. Tieleman and S.-J. Marrink (2008). "The MARTINI Coarse-Grained Force Field: Extension to Proteins." Journal of Chemical Theory and Computation **4**(5): 819 834.
Moon, C. P. and K. G. Fleming (2011). "Side-chain hydrophobicity scale derived from transmembrane protein folding into lipid bilayers." Proc Natl Acad Sci U S A **108**(25): 10174-10177.
Mulligan, C., C. Fenollar-Ferrer, G. A. Fitzgerald, A. Vergara-Jaque, D. Kaufmann, Y. Li, L. R. Forrest and J. A. Mindell (2016). "The bacterial dicarboxylate transporter VcINDY uses a

two-domain elevator-type mechanism." Nature Structural & Molecular Biology **23**(3): 256 263.

Oliver, R. C., J. Lipfert, D. A. Fox, R. H. Lo, S. Doniach and L. Columbus (2013). "Dependence of Micelle Size and Shape on Detergent Alkyl Chain Length and Head Group." PLoS ONE **8**(5): e62488.

Perez, A., J. A. Morrone, C. Simmerling and K. A. Dill (2016). "Advances in free-energy-based simulations of protein folding and ligand binding." Curr Opin Struct Biol **36**: 25-31.

Phillips, J., R. Braun, W. Wang, J. Gumbart, E. Tajkhorshid, E. Villa, C. Chipot, R. Skeel, L. Kale and K. Schulten (2005). "Scalable molecular dynamcs in NAMD." J Comp. Chem. **26**: 1781-1802.

Phillips, R., T. Ursell, P. Wiggins and P. Sens (2009). "Emerging roles for lipids in shaping membrane-protein function." Nature **459**(7245): 379-385.

Reyes, N., C. Ginter and O. Boudker (2009). "Transport mechanism of a bacterial homologue of glutamate transporters." Nature **462**: 880-885.

Ruan, Y., A. Miyagi, X. Wang, M. Chami, O. Boudker and S. Scheuring (2017). "Direct visualization of glutamate transporter elevator mechanism by high-speed AFM." Proceedings of the National Academy of Sciences **114**(7): 1584 1588.

Ryan, R. M., E. L. R. Compton and J. A. Mindell (2009). "Functional Characterization of a Na+-dependent Aspartate Transporter from Pyrococcus horikoshii." Journal of Biological Chemistry **284**(26): 17540-17548.

Silverstein, N., T. J. Crisman, L. R. Forrest and B. I. Kanner (2013). "Cysteine Scanning Mutagenesis of Transmembrane Helix 3 of a Brain Glutamate Transporter Reveals Two Conformationally Sensitive Positions." Journal of Biological Chemistry **288**(2): 964-973.

Sonntag, Y., M. Musgaard, C. Olesen, B. Schiøtt, J. V. Møller, P. Nissen and L. Thøgersen (2011). "Mutual adaptation of a membrane protein and its lipid bilayer during conformational changes." Nature Communications **2**(1): 304.

Tzingounis, A. V., C.-L. Lin, J. D. Rothstein and M. P. Kavanaugh (1998). "Arachidonic Acid Activates a Proton Current in the Rat Glutamate Transporter EAAT4." J. Biol. Chem. **273**(28): 17315-17317.

Verdon, G. and O. Boudker (2012). "Crystal structure of an asymmetric trimer of a bacterial glutamate transporter homolog." Nature Structural & Molecular Biology **19**(3): 355.

Wassenaar, T. A., K. Pluhackova, R. A. Böckmann, S.-J. Marrink and D. P. Tieleman (2014). "Going Backward: A Flexible Geometric Approach to Reverse Transformation from Coarse Grained to Atomistic Models." Journal of Chemical Theory and Computation **10**(2): 676 690.

Watson, M. C., E. G. Brandt, P. M. Welch and F. L. H. Brown (2012). "Determining biomembrane bending rigidities from simulations of modest size." Phys. Rev. Lett. **109**(2).

Yernool, D., O. Boudker, Y. Jin and E. Gouaux (2004). "Structure of a glutamate transporter homologue from *Pyrococcus horikoshii*." Nature **431**(7010): 811-818.

Zerangue, N., J. L. Arriza, S. G. Amara and M. P. Kavanaugh (1995). "Differential Modulation of Human Glutamate Transporter Subtypes by Arachidonic Acid." J. Biol. Chem. **270**(12): 6433-6435.